DESIGN AND IMPLEMENTATION OF A NOVEL CMOS-MEMS SINGLE PROOF-MASS TRI-AXIS ACCELEROMETER

Chih-Ming Sun[1], Ming-Han Tsai [1], and Weileun Fang[1,2]
[1]Nanoengineering and Microsystem Institute, [2]Power Mech. Eng. Dept,
National Tsing Hua University, Hsinchu, Taiwan

ABSTRACT

This study presents a novel single proof-mass tri-axis capacitive CMOS MEMS accelerometer to reduce the footprint of chip. A serpentine out-of-plane (Z-axis) spring is designed to reduce cross-axis error. A magnetic actuation for Z-axis self-test is also presented. The tri-axis accelerometer has been successfully implemented using TSMC 2P4M process and our in-house post-process. Measurement results show that sensitivities (non-linearity) of etch direction are 0.53mV/G (2.64%) of X-axis, 0.28mV/G (3.15%) of Y-axis, and 0.2mV/G (3.36%) of Z-axis. The cross-axis sensitivities range from 1% to 8.3%, and the measurement range is between 0.8~6G, respectively.

INTRODUCTION

The integration of smaller MEMS inertial sensor can find many applications in automobile industry, consumer electronics (e.g. digital camera, mobile phone, notebook, and video games), etc. Thus, the need of multi-axes (dual-axis or tri-axis) accelerometer is increased. Various batch fabrication technologies, such as surface micromachining [1], bulk micromachining [2], SOI process [3], and CMOS technology [4-6], have been reported to realize the MEMS accelerometers. As to the device design, the tri-axis MEMS accelerometer has been extensively investigated in [2-5]. In 2006, the integration of tri-axis MEMS accelerometer [7,8] has been exploited for video game motion-controller, named "Wii Remote" [9]. The multi proof-mass designs for in-plane and out-of-plane sensing are adopted in most reported monolithic multi-axis accelerometers [2-4]. The multi proof-mass accelerometer has the advantages of less cross-talk between sensing axes and relatively easier to design, however, larger chip size is required.

It is possible to reduce the size as well as the cost by implementing the tri-axes MEMS accelerometer using the single proof-mass design. For instance, as reported in [4,10], near 50% chip size can be reduced by the single proof-mass tri-axis accelerometer design. However, the complicated mechanical structures and sensing electrodes of the single proof-mass tri-axis accelerometer are critical design considerations. It is even challenge to design the single proof-mass tri-axis accelerometer using the existing CMOS process. This study presents a novel single proof-mass tri-axis capacitive CMOS MEMS accelerometer to reduce the footprint of chip. A serpentine out-of-plane (Z-axis) spring and sensing finger structures are designed to reduce the cross-axis sensitivity. In application, the accelerometer has been implemented using TSMC 0.35μm 2P4M CMOS process plus the present post-release technique.

DESIGN CONCEPT

Fig.1a shows the present tri-axis accelerometer consisting of one proof-mass, two supporting frames, and three sets of springs (named X-, Y-, and Z-spring) and sensing electrodes. These three sets of springs are designed only flexible in one axis. The exploded drawing in Fig.1b shows the proof-mass supported by Z-spring to form the Z-axis sensing element. Such Z-axis sensing element connects to a frame supported by Y-spring to form the Y-axis sensing element. Similarly, the Y-axis sensing element connects to a frame supported by X-spring to form the X-axis sensing element. These three parts form the three orthogonal sensing elements of the tri-axis accelerometer. The detail information of the tri-axis accelerometer design, including (1) Z-spring design, (2) sensing electrode for cross-axis decoupling design, and (3) out-of-plane magnetic actuation self-test design, is discussed as follows,

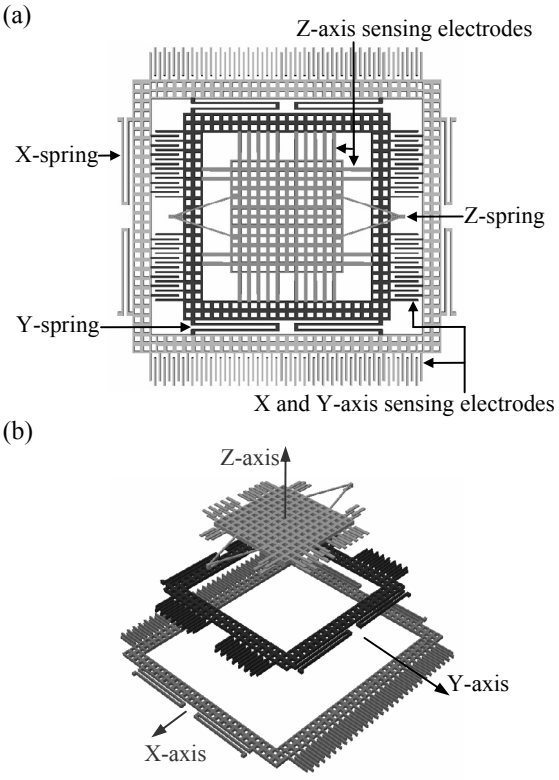

Figure 1 Design concept of single proof-mass tri-axis accelerometer, (a) top view, (b) exploded drawing of the sensing units for three different axes.

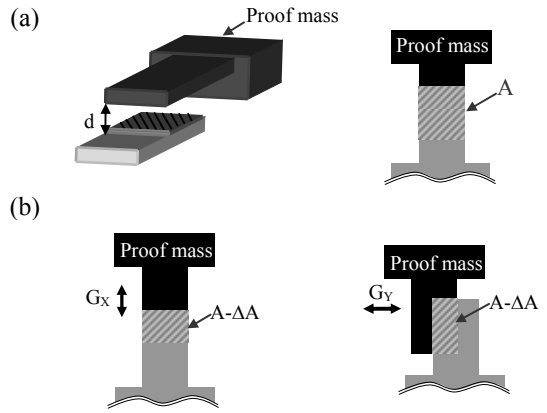

Figure 2 The overlap area of sensing electrodes (in dashed line) for Z-axis comb-finger, (a) ideal case without in-plane motions, and (b) real case with in-plane motions.

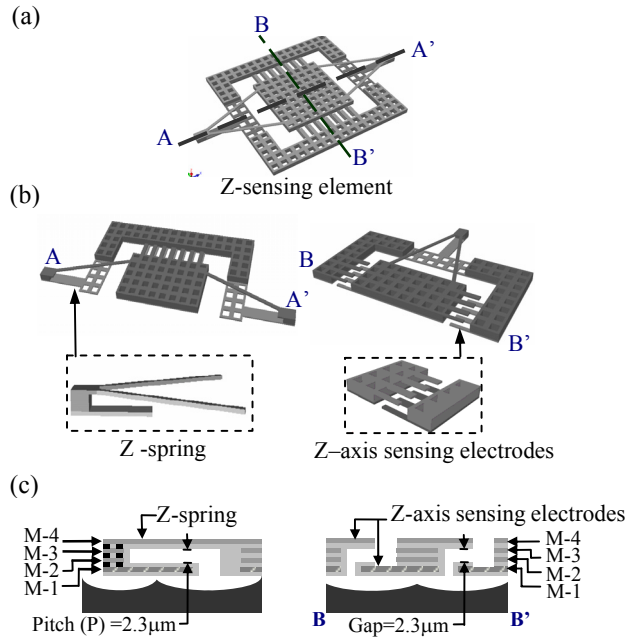

Figure 3 Design concept of Z-sensing element, (a) top view, (b) cross-section view of Z- spring and Z-axis sensing electrodes, and (c) structure layer of Z-spring and Z-axis sensing electrodes.

- **Z-spring design**

The cross-axis single coupling is the primary design consideration for the presented tri-axis accelerometer. The capacitance C between two parallel sensing electrodes varies with A/d, where A is the overlap area and d is the gap of these two electrodes. For instance, consider an ideal Z-axis sensing element in Fig.2a; the gap-closing capacitive sensing electrodes have a constant overlap area A (in dashed line). Thus, the capacitance change of Z-axis sensing electrodes is resulted from the variation of gap d caused by the inertial force in Z-axis. However, in the real application, the acceleration in X- or Y-axis will lead to the in-plane motion of the sensing electrodes, and further cause the change of overlap area ΔA as shown in Fig.2b. As a result, the Z-axis capacitance change will couple with the in-plane accelerations.

The cross-axis signal coupling can be reduced by spring design. It is straightforward to design and fabricate desirable planar X- and Y-springs using micro fabrication processes. On the other hand, it is challenge to realize a promising Z-spring for sensing decoupling. This study presents a novel Z-spring design to reduce the cross-axis signal coupling for Z-axis sensing element, as shown in Fig.3. Figure 3a shows the Z-axis sensing element. The illustrations in Fig.3b respectively show the cross-section views of Z-spring (AA'-section in Fig.3a) and Z-axis sensing fingers (BB' -section in Fig.3a). The novel serpentine CMOS MEMS Z-spring is a structure folded in the out-of-plane direction, and designed to increase the stiffness ratio of in-plane/out-of-plane. As shown in Fig.3c, the pitch (P=2.3μm) of the folded structure is realized by the sacrificial metal etching. As indicated in Fig.3b-c, the top structure (M-4) of folded Z-spring connects to proof-mass, and the bottom structure (M-1) of folded Z-spring connects to Y-supporting frame. The joint of top and bottom structures is formed by metal layers (M-3 and M-2) and vias. In this study, the out-of-plane stiffness of Z-spring is two orders smaller than its in-plane stiffness. The coupling of sensing signals between Z-axis and the in-plane axes is significantly suppressed. Moreover, the folded Z-spring also has the advantages of wide linear loading range, and the release of thin film residual stress of CMOS layers.

- **Sensing electrode design for cross-axis decoupling**

In addition to spring design, this study also presents the sensing electrode design to reduce the cross-axis signal coupling. As shown in Fig.4a, this study proposed the design of Z-axis sensing electrodes with different in-plane dimensions. The edge length of the bottom electrode (dashed line) is 1μm smaller than the top electrode. Thus, the in-plane motion of the electrodes induced by the X- or Y-axis acceleration will not lead to the change of overlap area (the 0.5μm edge length can tolerate in-plane acceleration), as indicated in Fig.4b. Only the Z-acceleration will lead capacitance change. Similarly, the in-plane sensing electrode also employs the same design concept to reduce the cross-axis coupling of X-axis and Y-axis sensing signals.

- **Out-of-plane magnetic actuation self-test**

A novel magnetic actuation design in Fig.5a was implemented for self-test of Z-axis sensing element. As shown in Fig. 5b, the wire coils formed by two aluminum layers (M-2 and M-3) and the permanent magnet (outside of the ceramic housing) were exploited to produce a magnetic force to drive the Z-axis accelerometer. As compare with the self-test by electrostatic actuation, the magnetic actuation has the following advantages: (1) no complicated electrical routing required, (2) smaller driving voltage, and (3) no actuation electrodes required.

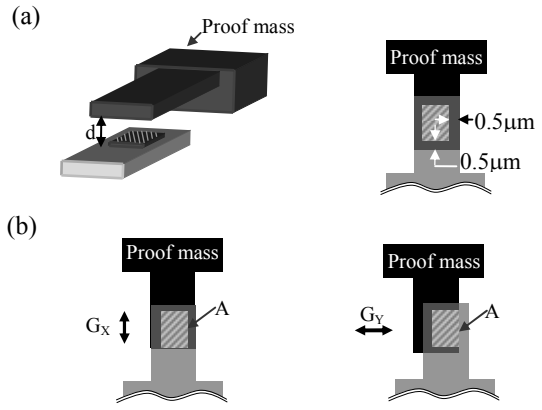

Figure 4 Overlap of the sensing electrodes(in dashed line) on comb-finger, (a) new Z-axis sensing electrodes design with different areas, and (b) the overlap sensing area A is not changed by the in-plane motions .

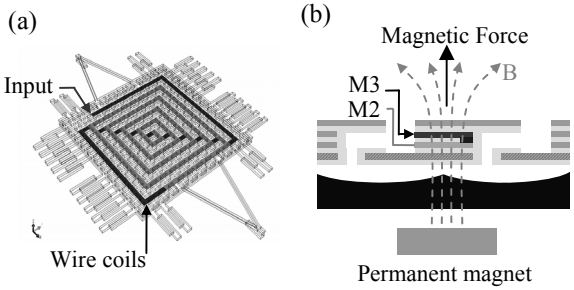

Figure 5 The Z-axis self-test design by magnetic actuation, (a) the magnetic coils prepared using two CMOS metal layers (M2 and M3 layers), and (b) magnetic force produced by magnetic coils and permanent magnet.

CMOS MEMS POST PORCESS

Figure 6 shows the present fabrication steps to realize a monolithic integrated single proof-mass tri-axis CMOS accelerometer. The two cross-section views respectively indicate the process steps for Z-spring (AA' cross section in Fig.3) and out-of-plane sensing comb-fingers (BB' cross section in Fig.3). The fabrication begins with the TSMC foundry service 0.35μm CMOS 2P4M process, as shown in Fig.6a. After that, the post CMOS processes consist of metal wet-etching, dielectric dry-etching, and bulk Si etching processes from the front-side of substrate are in Fig.6b-d.

As shown in Fig.6a, the pattern and stacking designs of metal films and tungsten vias are clearly observed. These metal films were exploited as sacrificial layers and sensing electrodes. The passivation layer was patterned to define the region for the following wet etching. As shown in Fig.6b, the H_2SO_4 and H_2O_2 solution was used to etch through the metal and tungsten vias [11, 12]. The passivation layer acted as a protection film during wet etching. In addition, the dielectric film distributed along the path of wet etching was also employed as the protection sidewall in this process.

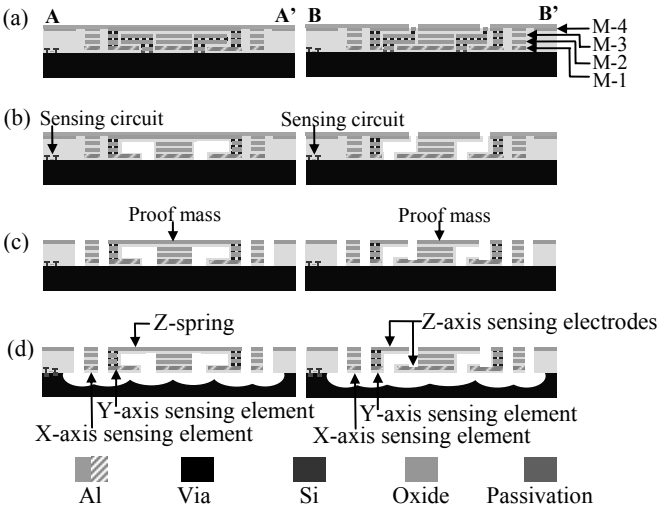

Figure 6 The fabrication steps of post-CMOS processes.

However, the dielectric blocks surrounded by sacrificial metal layers were fully released and then removed from substrate after the metal layers were etched away. Thus, (1) thickness and pitch of out-of-plane springs, and (2) the gap between top and bottom electrodes, were defined. After removing the top passivation layer, as illustrated in Fig.6c, the RIE was employed to etch dielectric SiO_2 layers (top metal layer M4 acted as etching mask) to define: (1) the shape of accelerometer, and (2) the gap between the stationary and the moving comb-fingers of in-plane accelerometers. Finally, the dry silicon isotropic etching using XeF_2 was used to release the accelerometers, as shown in Fig.6d.

EXPERIMENT AND RESULTS

This study has successfully demonstrated the tri-axis accelerometer using the process in Fig.6. The SEM micrograph in Fig.7 is a typical fabricated CMOS-MEMS single proof-mass tri-axis accelerometer (770μm×770μm). Near 50% chip footprint is reduced. The out-of-plane serpentine spring is clearly observed in zoom-in micrographs, as shown in Fig.7. The chip also contains CMOS circuits to form a standard two-stage cascode differential amplifier [13], which is employed to act as the capacitance readout IC. Fig.8 further shows the accelerometer chip after wire bonding and packaging. To calibrate the performance of present accelerometer, a commercial accelerometer was also packaged on the test board.

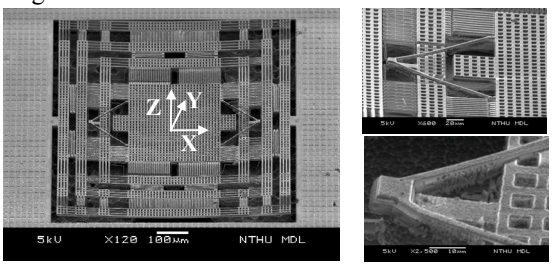

Figure 7 The SEM micrographs of single proof-mass tri-axis accelerometer, and the zoom-in of serpentine Z-spring.

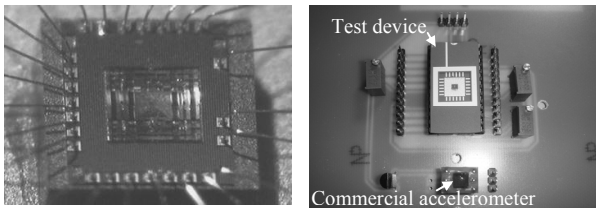

Figure 8 The accelerometer chip, (a) after wire bonding and packaged in ceramic housing, and (b) assemble on test board.

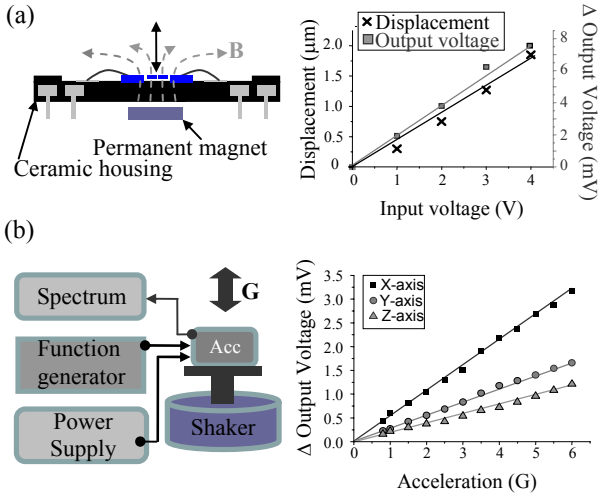

Figure 9 (a) The Z-axis self-test and the typical measured input voltage vs. static displacement and associated output sensing signal, and (b) the test setup to characterize the tri-axis accelerometer and the typical measured sensitivities.

Fig.9a shows experiment setup for the Z-axis self-test by magnetic actuation. The measurement results show the driving voltages (<5V) versus out-of-plane displacements as well as the associated output sensing-signal. The results demonstrated the feasibility of the magnetic actuation for Z-axis self-test. The test setup in Fig.9b was established to characterize the performance of accelerometer. The accelerometer was excited by the shaker. The misalignment of the shaker and accelerometer is used to measure the cross talk of the sensor. The excitation range provided by shaker is from 0.8G to 6G. Fig.9b shows the measured sensitivities of accelerometer are 0.53mV/G (X-axis), 0.28mV/G (Y-axis), and 0.2mV/G (Z-axis). The cross-axis sensitivity and non-linearity of accelerometer are respectively less than 8.3% and 4%. Table 1 summarizes the characteristics of accelerometer. Measurement results demonstrate the feasibility of the single proof-mass tri-axis accelerometer. Moreover, the serpentine Z-spring designs can reduce the cross-axis sensitivity.

CONCLUSIONS

This study presents a novel design of single proof-mass tri-axis capacitive CMOS MEMS accelerometer. To reduce the cross-axis sensitivity, the serpentine out-of-plane (Z-axis) spring and the special in-plane and out-of-plane sensing electrodes are designed. In addition, a magnetic actuation for Z-axis self-test is also presented. The tri-axis accelerometer has been successfully implemented using TSMC 2P4M process and our in-house post-process. Measurement results show that sensitivities (non-linearity) in etch direction are: 0.53mV/G (2.64%) of X-axis, 0.28mV/G (3.15%) of Y-axis, and 0.2mV/G (3.36%) of Z-axis. The cross-axis sensitivity ranges from 1% to 8.3%, and the measurement range is between 0.8~6G, respectively. In summary, the presented single proof-mass tri-axis CMOS MEMS accelerometer offers reasonable sensitivities and acceptable cross-axis sensitivity.

Table 1 Characterizations of the tri-axis accelerometer.

	Tri-axis accelerometer		
Sensing-axis	***X-axis***	***Y-axis***	***Z-axis***
Sensitivity (mV/G)	0.53	0.28	0.2
Non-linearity (%)	2.64	3.15	3.36
Resonant Freq. (KHz)	7.89	16.15	9.65
Cross-axis Sensitivity X(%)		< 7.46	< 8.05
Cross-axis Sensitivity Y(%)	< 1		< 2.88
Cross-axis Sensitivity Z (%)	< 1	< 8.33	

ACKNOWLEDGEMENTS

This project was (partially) supported by the NSC of Taiwan under grants 96-2628-E-007-008-MY3 and 95-2221-E-007-068-MY3. The authors would like to thank TSMC Ltd., and National Chip Implementation Center (CIC), Taiwan, for supporting the IC Manufacturing. The authors would also like to thank National Tsing Hua Universuty., and National Chiao Tung University. for providing the fabrication facilities.

REFERENCE

[1] K.H.L. Chau, S.R. Lewis, Y. Zhao, R.T. Howe, S.F. Bart, and R.G. Marcheselli, *Sensor and Actuator A*, **54**, pp 472-476, 1996.
[2] K. Kwon, and S. Park, *Sensors and Actuators A*, **66**, pp.250-255, 1998
[3] J. Chae, H. Kulah, and K. Najafi, *J. of.MEMS*, **14**, pp 235-241, 2005.
[4] M.A. Lemkin, M.A. Ortiz, N. Wongkomet, B.E. Boser, and J.H. Smith, *44th ISSCC 1997*, pp.202-203, 457.
[5] H. Qu, D. Fang, and H. Xie, *IEEE Sensors J.*, **8**, 2008, pp.1511-1518.
[6] H. Luo, G. Zhang, L.R. Carley, and G.K Fedder, *J. of. MEMS*, **11**, 2002, pp.188-195.
[7] Analog Device Inc., ADXL 330, http://www.analog.com
[8] *ST* Microelectronics LIS3L02, http://eu.st.com
[9] Nintendo Inc., http://www.nintendo.com
[10] M.A. Lemkin, B.E. Boser, D. Auslander, and J.H. Smith, *Transducer'97*, pp.1185-1188. 1997.
[11] C. Wang, M.-H. Tsai, C.-M. Sun, and W. Fang, *J. Micromech. Microeng* **, 17**, 2007, pp. 1275-1280.
[12] O. Paul, and H. Baltes, *Sensors and Actuators A*, **46/47**, no.1-3, 1995, pp. 143-146.
[13] J.M. Tsai, and G.K. Fedder, *IEEE MEMS'05*, 2005, pp. 630-633.